A strong tracking adaptive fading-extended Kalman filter for the state of charge estimation of lithium-ion batteries.

TAKYI-ANINAKWA, P., WANG, S., ZHANG, H., APPIAH, E., BOBOBEE, E.D. and FERNANDEZ, C.

2022

A strong tracking adaptive fading-extended Kalman filter for the state of charge estimation of lithium-ion batteries

Paul Takyi-Aninakwa[1] | Shunli Wang[1] | Hongying Zhang[1] | Emmanuel Appiah[1] | Etse Dablu Bobobee[1] | Carlos Fernandez[2]

1 School of Information Engineering, Southwest University of Science and Technology, Mianyang, China

2 School of Pharmacy and Life Sciences, Robert Gordon University, Aberdeen, UK

Correspondence

Shunli Wang, School of Information Engineering, Southwest University of Science and Technology, Mianyang 621010, China. Email: 497420789@qq.com

Funding information

Southwest University of Science and Technology, Grant/Award Numbers: 18zx7145, 17zx7110;
Environment Key Laboratory of Sichuan Province, Grant/Award Number: 18kftk03;
China Scholarship Council, Grant/Award Number: 201908515099;
National Natural Science Foundation of China, Grant/Award Number: 61801407

Summary

Lithium-ion batteries are widely used as rechargeable energy and power storage system in smart devices and electric vehicles because of their high specific energy, high power densities, etc. The state of charge (SOC) serves as a vital feature that is monitored by the battery management system to optimize the performance, safety, and lifespan of lithium-ion batteries. In this paper, a strong tracking adaptive fading-extended Kalman filter (STAF-EKF) based on the second-order resistor–capacitor equivalent circuit model (2RC-ECM) is proposed for accurate SOC estimation of lithium-ion batteries under different working conditions and ambient temperatures. The characteristic parameters of the established 2RC-ECM for the lithium-ion battery are identified offline using the least-squares curve fitting method with an average R-squared value of 0.99881. Experimental data from the hybrid pulse power characterization (HPPC) is used for the estimation and verification of the proposed STAF-EKF method under the complex Beijing bus dynamic stress test (BBDST) and the dynamic stress test (DST) working conditions at varying ambient temperatures. The results show that the established 2RC-ECM tracks the actual voltage of the battery with a maximum error of 28.44 mV under the BBDST working condition. For the SOC estimation, the results show that the proposed STAFEKF has a maximum mean absolute error (MAE) and root mean square error (RMSE) values of 1.7159% and 1.8507%, while the EKF has 6.7358% and 7.2564%, respectively, at an ambient temperature of -10C under the BBDST working condition. The proposed STAF-EKF delivers optimal performance improvement compared to the EKF under different working conditions and ambient temperatures, serving as a basis for an accurate and robust SOC estimation method with quick convergence for the real-time applications of lithium-ion batteries.

KEYWORDS

lithium-ion battery, second-order resistor–capacitor equivalent circuit model, state of charge estimation, strong tracking adaptive fading-extended Kalman filter, voltage traction

1 | INTRODUCTION

As the world progresses from fossil fuels toward electrification, the transport sector is becoming increasingly reliant on the development, manufacture, and supply of rechargeable batteries to replace carbon propulsion systems.[1] Rechargeable batteries, such as lithium-ion batteries, are gradually becoming the main power source and storage system.[2] They are preferred compared to batteries with other chemistries such as nickel-cadmium (NiCad), nickel-metal hydride (NiMH), and lead-acid due to their high energy and power densities. Also, they have other advantages, such as high voltage capacity, high recharge rate, low self-discharge rate, long cycle life, wide working temperature range, zero-emission of hydrogen gas, lightweight with compact size, high recyclability, and low hysteresis.[3-5]

The state of charge (SOC) is the ratio of the remaining useful capacity to the rated capacity of the lithium-ion battery, expressed as a percentage.[6] Accurate SOC estimation is of great significance to prevent damage to the battery and user. Also, it prevents over-charge and over-discharge as it has a functional relationship with the open-circuit voltage to inform the user about the necessary action and ensure safe operation and acceptable durability of lithiumion batteries.[7,8] The SOC indication in battery-powered vehicles works similarly to the fuel gauges in internal combustion engine-powered vehicles.[9] Even though the SOC is essential, it cannot be directly measured due to challenges like internal and external working conditions, cell size differences, aging characteristics, etc., of the lithium-ion battery.[10,11]

Currently, the frequently used methods for SOC estimation of lithium-ion batteries are classified into direct measurement-based such as the Ampere-hour (Ah) integral method[12] and open-circuit voltage method,[13] data-driven methods such as gated recurrent unit and long short-term memory neural networks,[14,15] and model-based methods such as Kalman filtering (KF) methods.[16] The circuit models commonly used in model-based estimation methods are the electrochemical model, the empirical model, the machine learning model, and the equivalent circuit model (ECM) to monitor its parameters and control the behavior of the lithium-ion battery.[17,18] The electrochemical model's working principle is based on the electrochemistry of the lithium-ion battery. It uses partial differential equations (PDEs) to characterize the response of internal cell electrochemical variables to an input current signal.[19,20] However, they are computationally complex due to the coupled PDEs and contain many influential model parameters.[21] The empirical model is established using a large amount of experimental data. However, due to parameter mismatch and cell differences, they cannot be applied to all working conditions in real-time applications.[22]

The ECM method trains the battery's model to simulate the internal characteristics of the lithium-ion battery.[23-25] The traditional KF and its advanced methods used for SOC estimation are applied to all types of batteries, provided that accurate input features such as load current, voltage, and temperature values are used.[26,27] Considering the complex and dynamic operational conditions of lithium-ion batteries, the SOC is estimated accurately by the optimization of the traditional model-based methods like the KF,[28] adaptive extended Kalman filter (AEKF),[29] extended Kalman filter (EKF),[5] particle filter (PF),[30] unscented Kalman filter (UKF),[8] H-infinity,[15] etc. These model-based methods are highly dependent on the ECM's ability to characterize the parameters of the battery. They are widely used by researchers due to their ability to estimate with high accuracy, good convergence, and with a smaller amount of data.[7,31]

The estimation methods that are easy to use and give optimal results compared to the KF are the EKF, UKF, and AEKF, which are the advanced methods for nonlinear systems such as lithium-ion batteries. The EKF is an optimized auto-recursive state estimation method that characterizes the internal dynamic states of the lithiumion battery.[32] For accurate SOC estimation studies carried out to enhance the performance of the battery management system (BMS), He et al.[32] established a fractional-order model using an adaptive genetic algorithm to characterize the dynamic responses of the lithium-ion battery based on a central difference KF to estimate the SOC at room temperature. It is observed that the fractional-order model works similarly to the second-order resistor– capacitor (2RC) ECM. Also, Wang et al.[33] and Cong et al.[34] used a composite ECM and the first-order Thevenin ECM to estimate the SOC of the lithium-ion battery using a spliced KF and an adaptive square root EKF, respectively. Yang et al.[35] used an improved EKF for the SOC estimation based on the first-order simulated annealing-particle swarm optimized ECM. Xu et al.[36] estimated the SOC and capacity based on the variation of

the model parameters and capacity of the battery using the AEKF method. A similar method of estimation is also found in Zhang et al.[37] using a one-way transmitted estimation of capacity and SOC with two different AEKF in succession using a first-order Thevenin ECM, which cannot fully characterize the polarization characteristics of lithium-ion batteries. The use of double estimation methods increases the computational complexity, and the adaptivity of the EKF is not robust enough to ensure accurate estimation. Yi et al.[38] combined the EKF with the Ah integral method based on the second-order Thevenin ECM for SOC estimation, which is prone to error accumulation even though it is easy to design and simple to use with the EKF, which also has its disadvantages. Also, a comparative study of the AEKF and UKF is conducted by Zhang et al.[39] for SOC estimation. Meanwhile, Zhao et al.[40] combined it with the AEKF only under the hybrid pulse power characterization (HPPC) working condition.

Due to the high nonlinearities of lithium-ion batteries, other state parameters such as state of health (SOH), state of energy (SOE), are state of power (SOP) are studied. Yang et al.[41] proposed a novel fuzzy adaptive cubature KF method for the co-estimation of the SOC and SOE. However, the inaccuracies and instabilities associated with the KF and EKF methods are not eliminated. Ma et al.[42] co-estimated the SOC and SOH based on a computationally complex fractional-order model with the multi-innovations UKF method. Xu et al.[43] proposed a fractional-order calculus for the co-estimation of the SOC and SOH based on a fractional-order ECM using a hybrid genetic algorithm/particle swarm optimization method. Wu et al.[44] estimate the SOP, which shows the peak power released or absorbed by the battery during its operation based on a Rint model. She et al.[45] based on the incremental capacity analysis method for the real-world estimation of the SOH for EV operation. Wang et al.[46] proposed a tree-based regression model for battery charging capacity diagnosis using charging rate, temperature, SOC, and accumulated driving mileage as the input data. However, among these state parameters, the SOC is the most significant function of the BMS. By accurately estimating it, the user can intuitively determine the critical condition of the battery by observing the changing rate of the SOC during the charge and discharge period. Also, the optimization accuracy of the proposed methods by these studies is not optimally obvious and has higher computational complexities. Furthermore, the robustness is not verified under complex working schemes and at varying ambient temperatures.

Due to technological advancement, artificial intelligence networks are prominently used for SOC estimation. Wang et al.[47] used an improved gated recurrent unit (GRU)-based transfer learning for small target sample sets for SOC estimation at high temperatures. Also, Huan et al.[48] proposed an improved whale optimization-AdaBoost-Elman algorithm, which solves the low generalization, local miniaturization, low prediction accuracy, and insufficient dynamics in the prediction process of a single feedforward neural network for SOC estimation at room temperature training and testing. Jia et al.[49] used a GRURNN-based momentum gradient method to optimize the weight of the network to estimate the SOC. However, the data learning process is complex, time-consuming, and requires high power and high-speed microprocessors to train the experimental data. Also, the human factors involved in the training process alter the certainty of the learning process and estimation accuracy. Due to these challenges, they are seldom used in engineering applications.[50] Studying the influence of temperatures in the operation of lithium-ion batteries, Wang et al.[51] developed a parameter identification method with the particle swarm optimization based on the constant current discharge test and estimated the SOC using the EKF at temperatures of 5 and 25C. The verification of their proposed method is carried out only at different discharge rates but not with different test conditions and low temperatures (0C and -10C), which highly influences the performance of lithium-ion batteries to show the robustness of the proposed method. Zhang et al.[52] estimated the SOC based on EKF and a regularized extreme learning machine (EKF-RELM) method that models the relationship between the lithium-ion battery's parameters and temperature. However, the study is conducted based on a time-varying temperature range, and their proposed methods were not verified under different working conditions.

In this paper, a strong tracking adaptive fading extended Kalman filter (STAF-EKF) method is proposed for SOC estimation based on the 2RC-ECM under varying ambient temperatures and working conditions. The characteristic parameters of the established 2RC-ECM are identified offline using the least-squares curve fitting method with high accuracy, 95% confidence bounds, and an average R-squared value of 0.99881. Then, the STAF factor is introduced into the recursive update of the posteriori error covariance matrix of the EKF to iteratively minimize the system's uncertainties and noise for an accurate and robust SOC estimation. Because temperature highly influences the performance of lithium-ion batteries, the SOC estimations of the STAF-EKF method are

conducted under the HPPC and the complex Beijing bus dynamic stress test (BBDST) working conditions at varying temperatures of 25C and -10C. Furthermore, the SOC estimation is carried out under the complex dynamic stress test (DST) working condition under varying ambient temperatures of 25C, 15C, 0C, and -10C to further verify the accuracy and robustness of the proposed method. The proposed STAF-EKF method effectively corrects the uncertainties and noise characterized by the nonlinearities in the SOC estimation of lithium ion batteries under different working conditions and ambient temperatures to improve the accuracy and robustness of the existing methods for real-time lithium-ion battery applications.

The rest of the paper is organized as follows: Section 2 introduces the mathematical analysis: the 2RC-ECM and its electrical behavior, the offline parameter identification method, the working principle of the proposed STAFEKF method, and the SOC performance evaluation metrics calculation. Section 3 describes the experimental analysis: the experimental test platform, the HPPC, BBDST, and DST experiment procedures, and the experimental verification of the 2RC-ECM. Then, the SOC estimation results for the STAF-EKF and the EKF methods are presented and evaluated using the maximum error (ME), mean absolute error (MAE), and root mean square error (RMSE) to show the performance improvement of the proposed method under different working conditions and ambient temperatures. Section 4 is the conclusion of this paper.

2 | MATHEMATICAL ANALYSIS

2.1 | The second-order resistor–capacitor equivalent circuit model

Compared to other types of rechargeable batteries, the lithium-ion battery has four primary components: positive and negative electrodes, an electrolyte, and a separator. The ECM has the advantages of simple calculation and characterization ability; therefore, it is the most widely used.[53] Some of the commonly proposed ECMs for lithium-ion batteries in hybrid electric vehicles (HEVs), plug-in hybrid electric vehicles (PHEVs), and battery electric vehicles (BEVs) studies are the Rint, Thevenin, Partnership for a New Generation of Vehicles (PNGV), general nonlinear (GNL), and resistor–capacitor (RC) circuit models.

The RC-ECM stands out because it is more capable of registering and monitoring the static and nonlinear characteristics of the battery.[50] The 1RC-ECM provides sufficient accuracy, easy implementation, and fast computation. However, it cannot fully simulate the dynamic characteristics of the lithium-ion battery accurately.[34,54] Therefore, an additional RC circuit can further simulate the charged and discharged states of the battery's nonlinearities with its dual-polarization making it a 2RC-ECM, for better dynamic performance and parameter characterization. The established 2RC-ECM of the lithium-ion battery used for this study is presented in Figure 1.

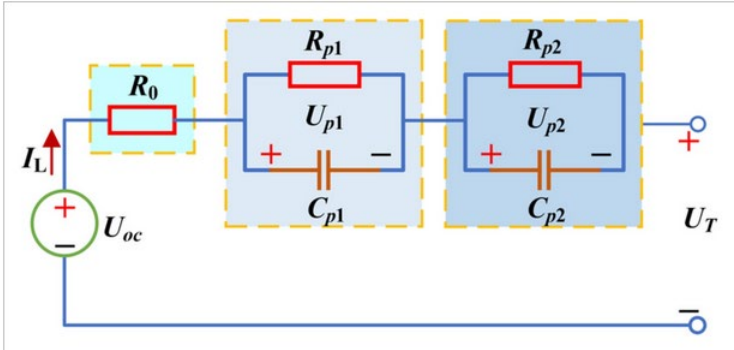

FIGURE 1 Second-order resistor–capacitor equivalent circuit model.

By analyzing the 2RC-ECM in Figure 1, its electrical behavior for the terminal voltage and load current is obtained based on Kirchhoff's circuit law as expressed in Equation (1).

$$\begin{cases} U_T = U_{oc} - I_L R_0 - U_{p1} - U_{p2} \\ I_L = C_{p1}\frac{dU_{p1}}{dk} + \frac{U_{p1}}{R_{p1}} = C_{p2}\frac{dU_{p2}}{dk} + \frac{U_{p2}}{R_{p2}} \end{cases} \quad (1)$$

In Equation (1), U_{oc} is the open-circuit voltage of the battery, which has a functional relationship with the SOC. U_T is the battery terminal voltage, and I_L is the load current flowing through the 2RC-ECM. R_0 is the internal ohmic resistance, and R_{p1} and R_{p2} are the internal electrochemical and concentration polarization resistances, respectively. C_{p1} and C_{p2} are the internal electrochemical and concentration polarization capacitances, respectively, of the lithium-ion battery. U_{p1} and U_{p2} are the resultant voltages drops across the electrochemical and concentration factors of the polarized resistors and capacitors, respectively. In this paper, it is assumed that the sign of the battery load current is negative when the battery is charging, and positive when it is discharging.

2.2 | Parameter identification of the 2RC-ECM

The offline identification method is used to identify the model parameters and reduce the computational time while ensuring the accurate calculation of the internal parameters of the battery. The parameter identification is carried out using the experimental results from the HPPC test. When the lithium-ion battery is at rest, there is no load current flowing through the battery. Then, aside from the electrochemical and concentration polarization effects, the voltage difference caused by the voltage drop at each time step is due to the ohmic resistance R_0, which is calculated as presented in Equation (2).

$$R_0 = \frac{(U_1 - U_2) + (U_4 - U_3)}{2I_L} \quad (2)$$

In Equation (2), I_L is the load current, U_1 is the opencircuit voltage U_{oc}, and U_2, U_3, U_4, and U_5 are the closed-circuit voltages used to calculate the R_0 value at each SOC level.

To express the voltage variation and polarization characteristics, the Uoc and closed-circuit voltages for SOC = 0.6 are presented, as presented in Figure 2.

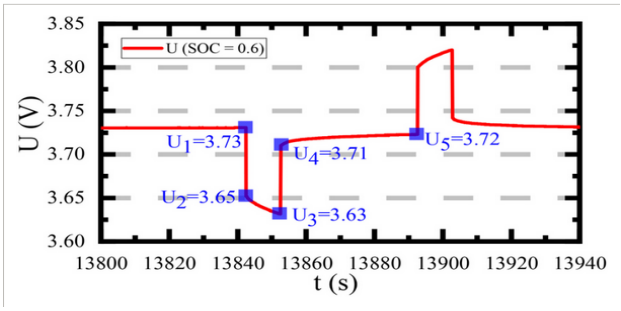

FIGURE 2 Characteristic time-varying charge-discharge voltage curve at SOC = 0.6.

Using the least-squares curve fitting method in MATLAB, the model's polynomial coefficients b, c, τ_1, and τ_2 are identified for each SOC variation (1.0, 0.9, 0.8, … 0.1) with 95% confidence bounds, and an average R-squared value of 0.99881. Then, the values of the electrochemical and concentration polarization parameters R_{p1}, R_{p2}, C_{p1}, and C_{p2} of the 2RC-ECM are calculated using their respective mathematical expressions presented in Equation (3).

$$\begin{cases} R_{p1} = \frac{b}{I_L} \\ R_{p2} = \frac{c}{I_L} \\ C_{p1} = \frac{\tau_1}{R_{p1}} \\ C_{p2} = \frac{\tau_2}{R_{p2}} \end{cases} \quad (3)$$

A seventh-order polynomial function is selected to eliminate the fluctuation with easy implementation and computation. The established seventh-order polynomial function of the 2RC-ECM parameters has an average R-squared value of 0.98996. The polynomial expression for the U_{oc}-SOC functional relationship for the simulation of the 2RC-ECM and SOC estimation is obtained, as presented in Equation (4).

$$U_{OC} = \begin{matrix} k_0 + k_1 \mathrm{SOC} + k_2 \mathrm{SOC}^2 + k_3 \mathrm{SOC}^3 + k_4 \mathrm{SOC}^4 \\ + k_5 \mathrm{SOC}^5 + k_6 \mathrm{SOC}^6 + k_7 \mathrm{SOC}^7 \end{matrix} \quad (4)$$

In Equation (4), k_0, k_1, k_2, k_3, k_4, k_5, k_6, and k_7 are the respective constant values for the seventh-order U_{oc}-SOC functional relationship with an R-squared accuracy of 0.9999.

2.3 | The strong tracking adaptive fading-extended Kalman filter (STAF-EKF) for SOC estimation

The ratio of the remaining useful capacity of the lithiumion battery to the maximum capacity is characterized as the SOC by the BMS. The expression of the SOC is presented in Equation (5).

$$\begin{cases} \mathrm{SOC}_k = 1 - \mathrm{DOD}_k = \frac{Q_{\max}}{Q_n} \times 100\% \\ \mathrm{SOC}_k = \mathrm{SOC}_0 - \frac{\int_0^k \eta I_L(k) dk}{Q_n} \end{cases} \quad (5)$$

In Equation (5), SOC_k is the current SOC estimated, and DOD_k is the depth of discharge at time step k. Q_{max} is the current available capacity measured, which may vary from the rated capacity of the battery due to aging and cyclic effects, and Q_n is the rated capacity of the battery given by the manufacturer. SOC_0 is the initial SOC estimated value, η is the Coulombic efficiency coefficient defined as 1 in this study, and $I_L(k)$ is the load current at time step k, assuming charging is negative and discharge is positive.

The EKF applies partial derivative and the first-order Taylor series expansion to the system's state-space equation to linearize the nonlinearities of lithium-ion batteries for SOC estimation.[37] It is an optimal regression data processing method over the traditional KF but possesses the limitation of estimating with a first-order accuracy at a high level of uncertainty and noise.[32] It estimates the state value of the next time step $k + 1$ using the measurements of the previous $k - 1$ and present time step k. The state-space equation of the EKF method is presented in Equation (6).

$$\begin{cases} x_k = A_k x_{k-1|k-1} + B_k u_k + w_k \\ y_{k+1|k} = C_k x_k + v_k \\ w_k \sim N(0, Q_k) \\ v_k \sim N(0, R_k) \end{cases} \quad (6)$$

The matrices of A_k, B_k, C_k, and u_k for the state-space equation are expressed in Equation (7).

$$A_k = \begin{bmatrix} 1 & 0 & 0 \\ 0 & \exp\left(-\frac{\Delta k}{\tau_1}\right) & 0 \\ 0 & 0 & \exp\left(-\frac{\Delta k}{\tau_2}\right) \end{bmatrix}$$

$$B_k = \begin{bmatrix} -\eta \bullet \Delta k / Q_n \\ R_{p1}\left(1 - \exp\left(-\frac{\Delta k}{\tau_1}\right)\right) \\ R_{p2}\left(1 - \exp\left(-\frac{\Delta k}{\tau_2}\right)\right) \end{bmatrix}$$

$$C_k = \begin{bmatrix} \frac{dU_{oc}}{d\,\mathrm{SOC}_k} & -1 & -1 \end{bmatrix}$$

$$u_k = I_L \quad (7)$$

In Equation (7), x_k is the state equation, and y_k is the output measurement equation at present step k. A_k is the state-transition matrix, which is applied to the state x_{k-1}. B_k is the control-input matrix, which is applied to the control-input vector u_k, and C_k is the measurement matrix at present time step k, which maps the state-space into the measured space. I_L is the load current of the lithium-ion battery and Δk is the sampling time interval. w_k and v_k are the system noise and measurement noise, which are assumed to be zero-mean Gaussian white noises with covariance matrices Q_k and R_k, respectively.

The traditional EKF used for SOC estimation is inherently affected by uncertainties and system noise. The STAF filter is introduced to reduce these effects to achieve accurate and robust estimates in the posteriori error covariance matrix calculation during the measurement update. The flowchart of the proposed STAF-EKF for the SOC estimation is presented in Figure 3.

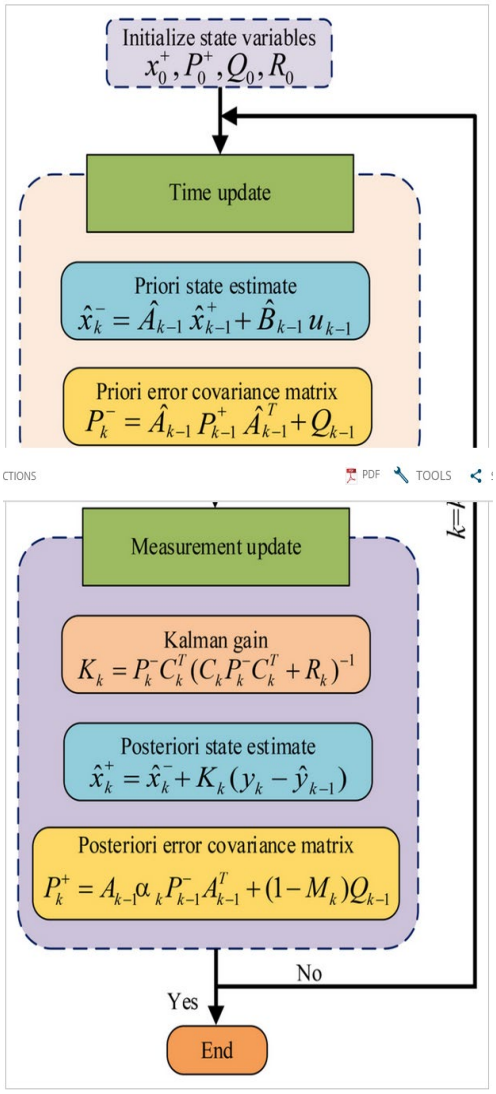

FIGURE 3 Flowchart of the proposed STAF-EKF method.

Firstly, an adjustment factor α_k $(0 \le \alpha_k \le 1)$ is introduced to eliminate the uncertainty effects in the posteriori error covariance matrix in the measurement update step. Secondly, M_k is the adjustment matrix for the system's noise covariance matrix. Its mathematical expressions are presented in Equation (8).

$$P_k^+ = A_{k-1}\alpha_k P_{k-1}^- A_{k-1}^T + (1 - M_k)Q_{k-1} \quad (8)$$

$$M_k = f(x) = \begin{cases} 1, \mid S_k \leq 1 \\ S_k = \frac{tr(P_k)}{tr(Z_k)}, \mid S_k > 1 \end{cases}$$

$$\begin{cases} P_k = T_k - \beta R_k - C_k \Gamma_k \Gamma_k^T C_k^T Q_{k-1} \\ Z_k = C_k A_{k-1} P_{k-1} A_{k-1}^T C_k^T \end{cases}$$

$$T_k = f(x) = \begin{cases} \gamma_1 \gamma_1^T, k \leq 1 \\ \frac{\rho T_{k-1} + \gamma_k \gamma_k^T}{1+\rho}, k > 1 \end{cases}$$

In Equation (8), T_k is the residual covariance matrix, ρ is the forgetting factor, which is optimally tuned within $0 < \rho \leq 1$, and β is the weakening factor, which is optimally tuned as $\beta \geq 1$ based on the extent of mismatch and current outcome of the estimated SOC compared to the actual SOC. Γ_k and γ_k are the noise adjustment and posteriori distribution matrices, respectively.

The iterative calculation of the STAF-EKF uses the adjustment factor αk and matrix Mk in Equation (8) to adjust the uncertainties and the system noise, respectively, to robustly characterize the nonlinearities of the lithium-ion battery for accurate real-time SOC estimation. Meanwhile, all other parameters of the traditional EKF, such as the values of the system noise, and measurement noise remain the same.

2.4 | Performance evaluation of the EKF and STAF-EKF methods for SOC estimation

In this paper, to critically evaluate the performance of both methods for SOC estimation, error metrics are employed. The error metrics used in this paper are the maximum error (ME), the MAE, and the RMSE. Their mathematical expressions of these metrics are presented in Equation (9).

$$\begin{cases} E_k = y_k - \hat{y}_k \\ \mathrm{ME} = \max_k 1, 2, \ldots, n(E_k) \\ \mathrm{MAE} = \frac{1}{n}\sum_{k=1}^{n} |y_k - \hat{y}_k| \\ \mathrm{RMSE} = \sqrt{\frac{1}{n}\sum_{k=1}^{n} (y_k - \hat{y}_k)^2} \end{cases} \quad (9)$$

In Equation (9), y_k is the actual SOC of the battery system, $\hat{y}_k$ is the estimated SOC by both methods, E_k is the error value between the estimated and the actual SOC at time step k, and n is the total number of the data sequence. The ME is the maximum divergence or error value in the error data sequence. The RMSE is the root mean square error, which shows how dispersed the error is away from the mean.

3 | EXPERIMENTAL ANALYSIS

3.1 | Experimental test platform

The NMC70Ah (nickel manganese cobalt oxide) lithiumion battery used for the experiment has a rated voltage of 4.2 V and a capacity of 70 Ah. It has nickel manganese cobalt as the cathode electrode and natural graphitic carbon with metallic backing as the anode electrode. The basic technical information of the lithium-ion battery is presented in Table 1.

TABLE 1 Basic technical information of the lithium-ion battery (NMC70Ah).

Parameter	Value	Parameter	Value
Nominal capacity	70 Ah	Standard load current	70 A
Nominal voltage	4.2 V	Maximum cut-off load current	100 A
Maximum cut-off voltage	4.5 V	Minimum cut-off load current	100 A
Minimum cut-off voltage	2.5 V	Dimensions: l × w × h	148 × 33 × 93 (mm)

The battery test equipment is a Neware battery test system (BTS-4000), which has a maximum load current of 100 A, a range of charge and discharge voltage of 25~100 V, and a maximum charge and discharge power of 12 kW. The temperature test equipment is a DGBELL BTT-331C. The experimental test platform is presented in Figure 4.

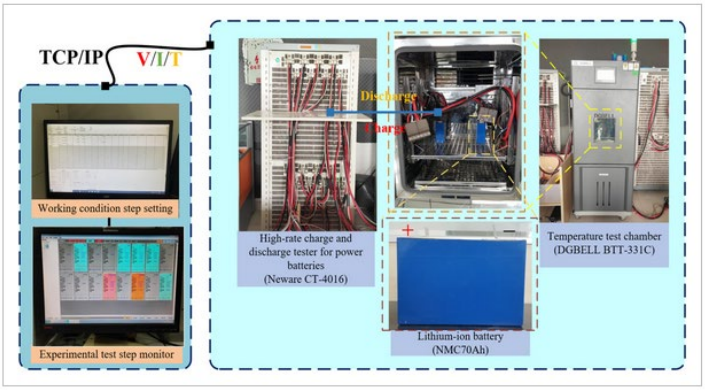

FIGURE 4 Experimental text platform

Figure 4 shows the charging and discharging experimental test platform established to obtain the parameters such as the battery terminal voltage and load current for both working conditions. It mainly consists of the charge-discharge control circuit, signal detector, circuit measurement system, electronic load, temperature test equipment, direct load current power supply to the lithium-ion battery, and a computer for setting and monitoring working steps. The main function of this experimental platform is to obtain the time-varying charge-discharge characteristics (load current, voltage, capacity, energy, etc.) of the lithium-ion battery for the proposed working condition. The battery data for each programmed working time step is stored during the experimental test. Firstly, the computer is used to input and send steps commands of the working condition through the electronic load of the serial port, which are the charging, discharging, and resting time steps. During an experimental test, the predefined steps are switched between the charging, discharging, and rest states with time, which can be monitored to know the status and performance of the test. Meanwhile, the experimental test results, such as the time-varying current, voltage, capacity, energy, and temperature of the lithium-ion battery for different temperatures and working conditions are graphically displayed and stored on the monitor of the general-purpose computer for each test. Finally, the experimental data is retrieved using the peripheral inter-connected data acquisition cable and processed. The charged and discharged state current, voltage, and temperature data values are used for the state estimation.

3.2 | The experimental procedure for the HPPC, BBDST, and DST working conditions

3.2.1 | HPPC working condition

The HPPC test is used to measure the pulse capability of lithium-ion batteries under varying sequential DOD levels for different time intervals. It is conducted to obtain its dynamic characteristics, and then the battery model parameters are calculated. For the HPPC test, first, the battery is charged with a 1 C/70 A constant load current and constant voltage. Then, the battery is rested for 40 min to ensure electrochemical and thermal equilibrium before the next test profile. A 10 s discharge pulse is conducted using a 1 C load current rate. After that, it rested for 40 s. A 10 s charge pulse is initiated at a 1 C load current rate and rested afterward for 40 s. The next cyclic HPPC is conducted on the lithium-ion battery after a 6 h rest period. The ten (10) SOC levels are selected from 0.1 to 1.0 at an interval of 0.1. The corresponding U_{oc} value for each SOC level is accurately measured before the start of the next HPPC test profile by the test system. The corresponding time-varying terminal voltages and load current characteristics of the HPPC test obtained for temperatures of 25C and -10C are presented in Figure 5.

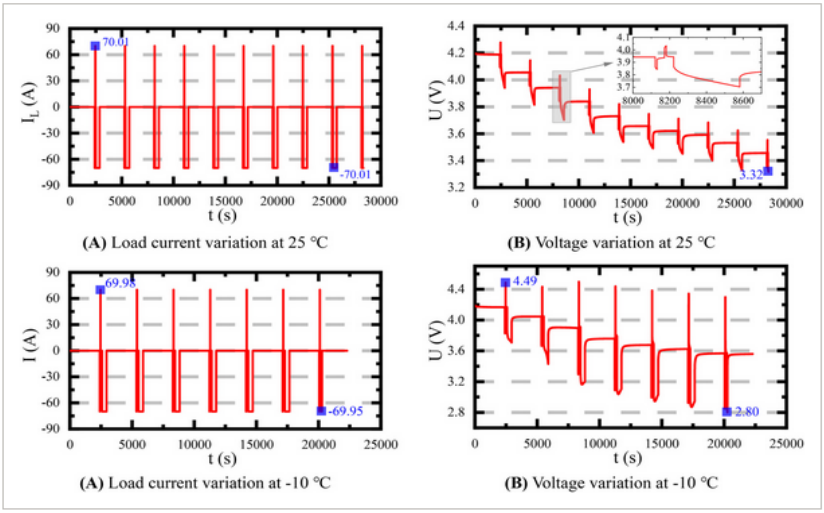

FIGURE 5 Time-varying load current and terminal voltage curves under the HPPC working condition at varying ambient temperatures.

3.2.2 | BBDST working condition

The complex BBDST working condition is conducted and obtained by processing the data collected from the start, acceleration, slide, brake, rapid acceleration, and stop of the Beijing bus. In a real-time application, the power at each step is reduced to simulate the Beijing bus's working condition. The complex working steps of the Beijing bus are presented in Table 2.

TABLE 2 Complex working steps of the Beijing bus.

Step	P_c(W)	Step time(s)	Total time(s)	Working Status
1	37.5	21	21	Start
2	72.5	12	33	Acceleration
3	4.5	16	49	Slide
4	-15	6	55	Brake
5	37.5	21	76	Acceleration
6	4.5	16	92	Slide
7	-15	6	98	Brake
8	72.5	9	107	Acceleration

9	92.5	6	113	Rapid acceleration
10	37.5	21	134	Acceleration
11	4.5	16	150	Slide
12	-15	6	156	Brake
13	72.5	9	165	Acceleration
14	92.5	6	171	Rapid acceleration
15	37.5	21	192	Acceleration
16	4.5	16	208	Slide
17	-35	9	217	Brake
18	-15	6	229	Brake
19	4.5	71	300	Stop

The time-varying load current and terminal voltage curves under the complex BBDST working condition for temperatures of 25C and -10C are presented in Figure 6.

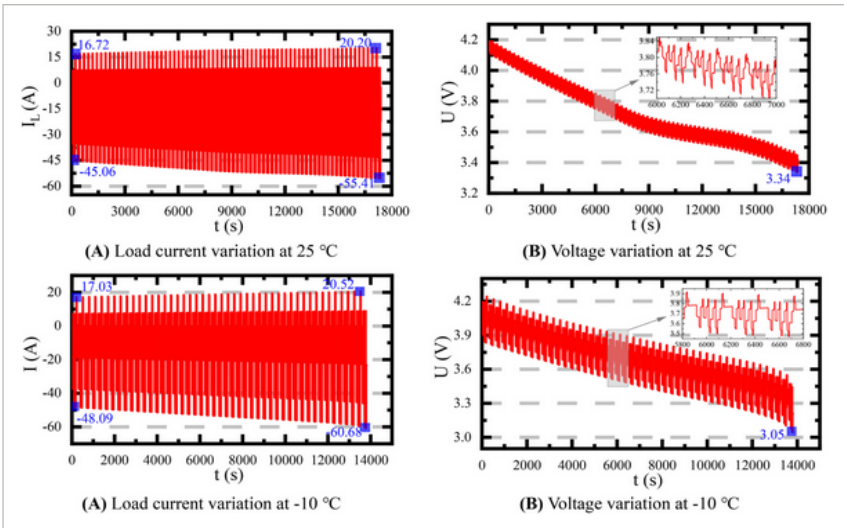

FIGURE 6 Time-varying load current and terminal voltage curves under the BBDST working condition at varying ambient temperatures.

3.2.3 | DST working condition

As a complex working condition, the DST is self-defined. The test procedures for conducting the DST under varying temperatures to obtain the experimental data, including the load current and voltage, for each temperature variation used for SOC estimation, are described as follows:

(i) The battery is charged to a maximum terminal voltage of 4.20 V with a constant current (CC) of 1 C for 30 min. Then, it is charged with a constant voltage (CV) until the current rate drops to 0.5 C for 4 min.

(ii) After charging is completed, the battery is rested to ensure electrochemical and thermal equilibrium before the next test cycle for 30 s, where the battery's voltage is equivalent to open-circuit voltage.

(iii) A CC discharge is carried out at a rate of 0.5 C for another 2 min. Then, the battery is rested for 30 s.

(iv) The battery is discharged at a CC rate of 1 C for another 4 min.

Steps (ii) to (iv) are repeated until the minimum cut-off terminal voltage is reached, which is mainly dependent on the temperature of the test. The load current and voltage variation curves for varying temperatures of 25C, 15C, 0C, and -10C are presented in Figure 7.

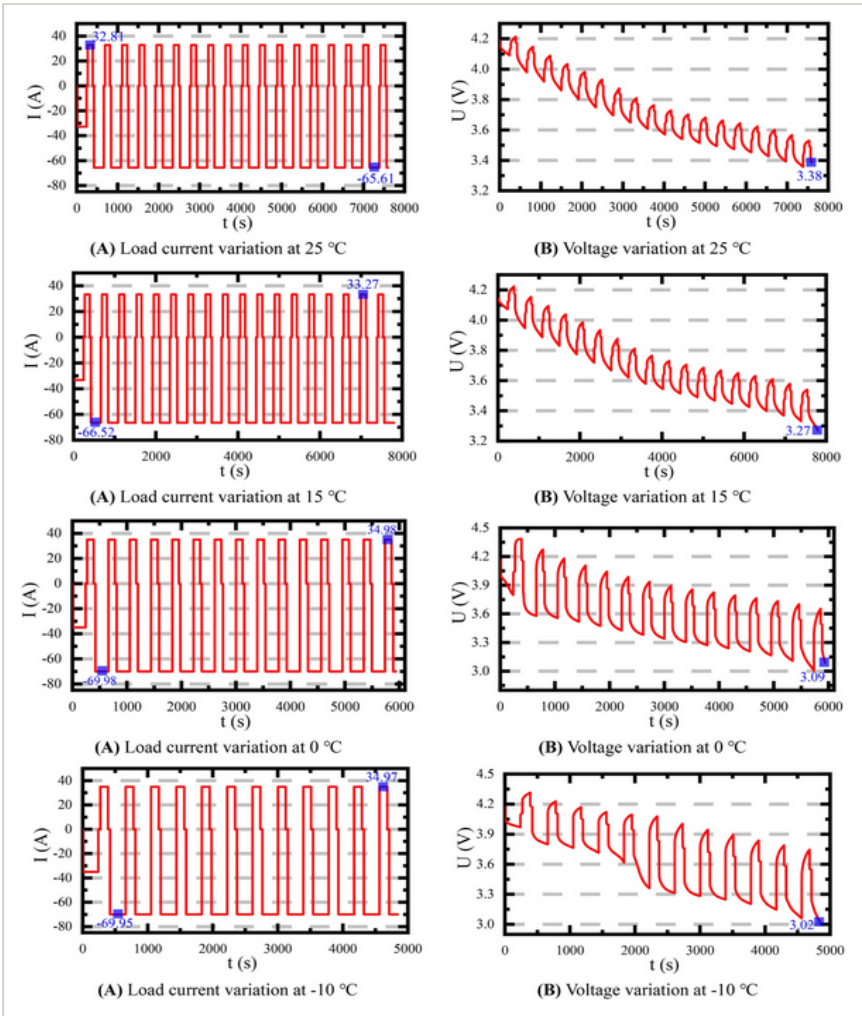

FIGURE 7 Time-varying load current and terminal voltage curves under the DST working condition at varying ambient temperatures.

3.3 | Experimental verification of the 2RC-ECM

From the experimental results of the BBDST experiment, the time-varying current and terminal voltage values obtained are used to verify the effectiveness and accuracy of the established 2RC-ECM in robustly simulating the dynamic characteristics of lithium-ion batteries in Simulink/MATLAB for real-time application. The model's time-varying output voltage is compared with the actual terminal voltage under the BBDST working condition, as presented in Figure 8.

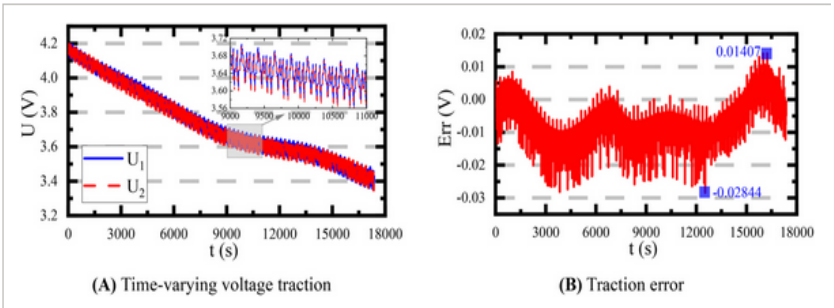

FIGURE 8 Time-varying voltage traction result of the 2RC-ECM under the BBDST working condition.

Figure 8 shows the experimental verification result for the comparison between the simulated voltage by the 2RC-ECM and the actual battery terminal voltage under the BBDST working condition. In Figure 8A, U_1 is the actual battery terminal voltage, and U_2 is the simulated voltage output by the established 2RC-ECM. Figure 8B shows the time-varying traction error of the simulated voltage by the 2RC-ECM (U_2) from the actual battery terminal voltage (U_1). From the result, the simulated voltage is observed to have a good track of the actual terminal voltage, resulting in an absolute ME value of 28.44 mV and an MAE value of 13.93 mV. By analyzing the error between the two voltages, a low margin error is observed at the early stage, and in the mid-stage, it increases due to the drift of the load current during the discharge cycles. However, it potentially converges at the later stage of the traction process with increasing time to adequately characterize lithium-ion batteries in real-time applications toward the end of the full discharge cycles.

3.4 | The STAF-EKF and EKF methods for SOC estimation

The proposed STAF-EKF is used for the SOC estimation and compared with the EKF under the HPPC working condition at temperatures of 25C and -10C. The SOC estimation results for both methods are presented in Figure 9.

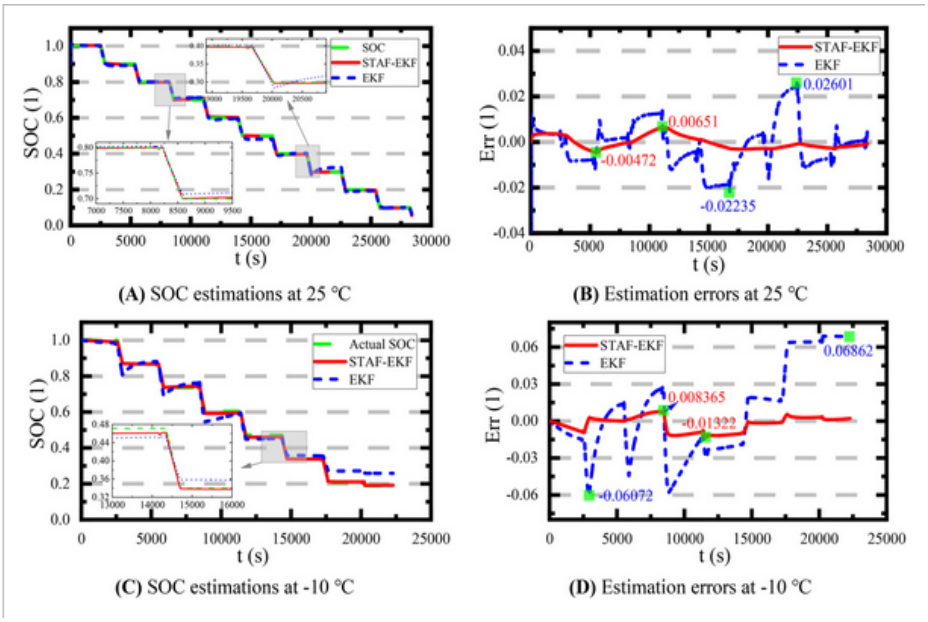

FIGURE 9 SOC estimation results using the STAF-EKF methods under the HPPC working condition at varying temperatures.

Figures 9A,C show the estimated SOCs by the STAFEKF and EKF in comparison with the actual SOC of the lithium-ion battery under the HPPC working condition at varying temperatures of 25C and -10C. Figures 9B, D show the SOC estimation error for both methods at a temperature variation of 25C and -10C, respectively, which is calculated independently by subtracting the estimated SOC from the actual SOC at each time step. The results show that at temperatures of 25C and -10C, the STAF-EKF has optimal accuracy with ME values of 0.651% and 1.322%, respectively. Meanwhile, the accuracy of the EKF is low, with ME values of 2.601% and 6.862% at 25C and -10C, respectively. For both temperature variations, it can be observed that the STAF-EKF has a quicker initial convergence to the actual SOC compared to the EKF. Also, its adaptability to the actual SOC for the entire estimation process is more robust and optimal than the EKF, which diverges, especially under the temperature of -10C due to its instability and high-capacity discharge of the lithium-ion battery.

A verification study of the proposed STAF-EKF with the EKF is conducted and analyzed under the complex BBDST working condition at varying temperatures of 25C and -10C. The SOC estimation results for both methods are presented in Figure 10.

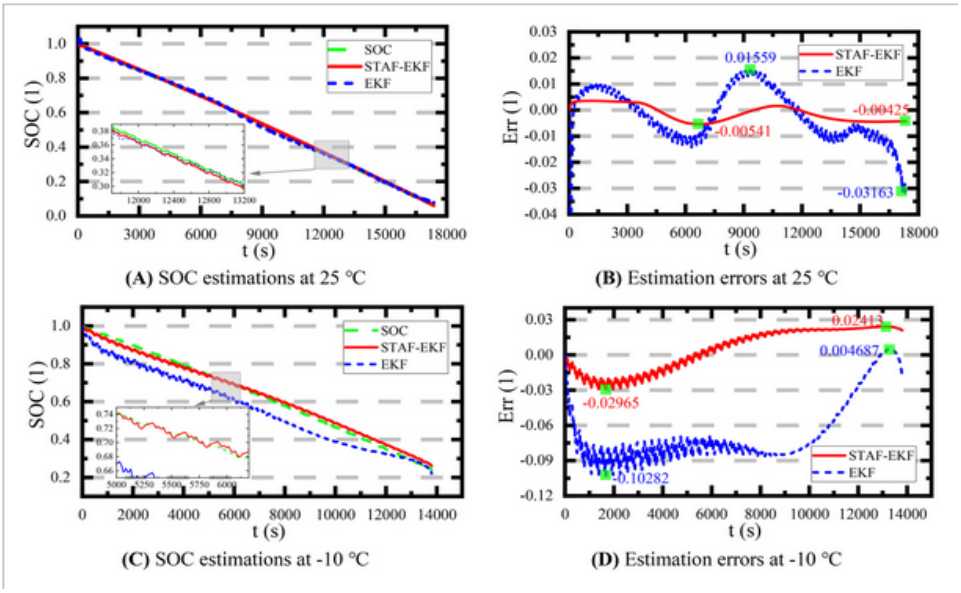

FIGURE 10 SOC estimation results using the STAF-EKF and EKF methods under the complex BBDST working condition at varying temperatures.

Under the complex BBDST working condition, both methods in Figures 10A,D show similar differences in estimation accuracy and robustness for both temperature variations. In Figures 10B,D, the STAF-EKF has optimal accuracy with ME values of 0.541% and 2.965% at temperatures of 25C and -10C, respectively. Meanwhile, at temperatures of 25C and -10C, the EKF estimations have high ME values of 3.163% and 10.282%, respectively. These error results show that the STAF-EKF converges faster at the initial estimation due to strong trackability and ensures robust SOC estimations for the entire process. Meanwhile, the convergence of the EKF is slow at the initial stage. It has divergence at the end of the estimation process due to the high level of capacity discharge of the lithium-ion battery under both temperature variations.

Because of the temperature effect on lithium-ion batteries, further verification studies of the proposed STAF-EKF compared with the EKF are conducted and analyzed under the complex DST working condition at varying temperatures of 25C, 15C, 0C, and -10C. The SOC estimation results for both methods at these varying temperatures are presented in Figure 11.

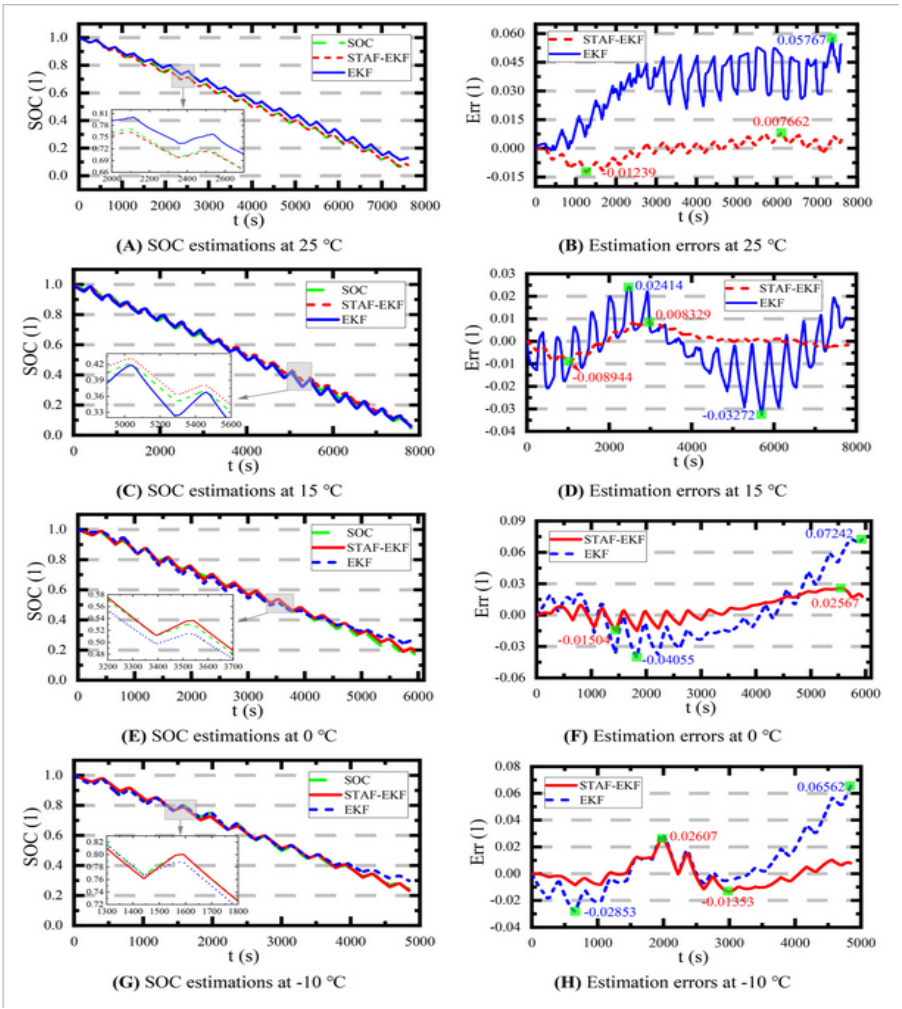

FIGURE 11 SOC estimation results for using the STAF-EKF and EKF methods under the complex DST working condition at varying temperatures.

In Figure 11, it can be observed that the STAF-EKF has better estimation accuracy compared to the EKF under the complex DST working condition and all temperature variations. The STAF-EKF optimally estimates with ME values of 1.239%, 0.894%, 2.560%, and 2.853% at temperatures of 25C, 15C, 0C, and -10C, respectively. Meanwhile, at the same temperature variations, the EKF estimates the SOC with ME values of 5.767%, 3.272%, 7.242%, and 6.562% while lagging with high noise and divergence from the actual SOC. Furthermore, the STAF-EKF possesses quick convergence to the actual SOC compared to the estimations using the EKF method. These estimation results show the strong trackability of the proposed method to the actual SOC of the lithium-ion battery.

The SOC estimation performance for the STAF-EKF and EKF methods is evaluated using the MAE and RMSE metrics under the three working conditions and temperature variations, as presented in Table 3.

TABLE 3 Performance evaluation using the STAF-EKF and EKF methods for SOC estimation.

Working conditions	Estimation temperatures	Evaluation metrics	STAF-EKF	EKF	Performance improvement
HPPC	25°C	MAE	0.2460%	1.1369%	78.36%
		RMSE	0.2812%	1.6672%	83.13%
		Estimation time	33.56 s	34.01 s	1.32%
	-10°C	MAE	0.4928%	3.0146%	83.65%
		RMSE	0.6389	3.7215%	82.83%
		Estimation time	33.24 s	35.18 s	5.51%
BBDST	25°C	MAE	0.2984%	0.8755%	65.92%
		RMSE	0.3332%	1.0465%	68.16%
		Estimation time	19.89 s	21.09 s	5.69%
	-10°C	MAE	1.7159%	6.7358%	74.53%
		RMSE	1.8507%	7.2564%	74.50%
		Estimation time	25.57 s	25.70 s	0.51%
DST	25°C	MAE	0.3910%	3.1689%	87.66%
		RMSE	0.4917%	3.5172%	86.02&
		Estimation time	21.02s	22.86 s	8.05%
	15°C	MAE	0.3193%	0.9857%	67.61%
		RMSE	0.4173%	1.2282%	66.02%
		Estimation time	16.89 s	17.63 s	4.20%
	0°C	MAE	0.9546%	2.2199%	57.00%
		RMSE	1.2274%	2.8304%	56.64%
		Estimation time	13.58 s	14.30 s	5.03%
	-10°C	MAE	0.7073%	1.6013%	55.83%
		RMSE	0.8776%	2.1793%	59.73%
		Estimation time	16.90 s	15.65 s	-7.99%

In Table 3, it can be observed that the STAF-EKF has optimal performance compared to the EKF, with lower error values and a high percentage of performance improvement, showing its robustness and accuracy.

But not compared to the complex BBDST working condition, the STAF-EKF is observed to estimate more accurately and has a better performance improvement under the HPPC. Also, it can be observed that the maximum MAE and RMSE values of 1.7159% and 1.8507% for the STAF-EKF and 6.7358% and 7.2564% for the EKF, respectively, occurred under the BBDST working condition at a temperature of -10C. It means the BBDST working conditions tend to be challenging because of the ambient temperature effect on the lithium-ion battery, but the STAF-EKF estimates with satisfactory accuracy. Even though the STAF-EKF is highly robust, under the DST working condition, its performance improvement of the SOC estimation by the EKF tends to reduce with decreasing temperature using the MAE metric. Also, under this working condition, the least overall performance improvement for both MAE and RMSE occurs at a temperature of 0C. However, it tracks and adapts to the nonlinear characteristics, enhances the certainty, and minimizes the noise effect, which causes inaccuracies in the SOC estimation of the EKF for the BMS of lithiumion batteries in real-time applications under various working conditions and temperatures. It can be observed that the STAF-EKF has an overall better performance compared to the EKF employing the estimation time due to its ability to recursively estimate the optimal SOC values with minimized computational requirements using the forgetting and weakening factors. However, at a temperature of -10C under the complex DST working condition, it can be observed that the estimation time of the STAF-EKF is higher than the EKF, which may be due to other nonlinearities.

4 | CONCLUSION

In this paper, a STAF is proposed in the EKF method to correct the effects of the uncertainties introduced by the posteriori error covariance and system noise to improve the SOC estimation accuracy based on the 2RC-ECM. The characteristic parameters of the established 2RC-ECM are identified offline using the least-squares curve fitting method with 95% confidence bounds and an average R-squared value of 0.99881. The accuracy and

robustness of the proposed STAF-EKF for SOC estimation are verified under the HPPC, the complex BBDST, and DST working conditions at varying ambient temperatures and compared with the EKF. The time-varying voltage traction results show that the 2RC-ECM accurately simulates the dynamic characteristics of the lithium-ion battery with a ME value of 28.44 mV under the complex BBDST working condition. For the SOC estimation, the results show that the proposed STAF-EKF has a maximum MAE and RMSE values of 1.7159% and 1.8507%, and the EKF has 6.7358% and 7.2564%, respectively, at an ambient temperature of -10C under the BBDST working condition. Also, it can be observed that the STAF-EKF has quick convergence and estimation time compared to the EKF. The STAF-EKF method has a strong correction of the uncertainty and system noise to prevent filter divergence to effectively estimate the SOC of lithium-ion battery for accurate SOC estimation in real-time applications in BMSs of EVs. It can be observed that the accuracy of the established 2RC-ECM is over 20 mV due to the lack of hysteretic characterization, which will be the focus of our future research work. Also, using the proposed STAF-EKF for the SOH estimation of lithium-ion batteries based on the hysteresis-compensated 2RC-ECM.

ACKNOWLEDGMENT

The work is supported by the National Natural Science Foundation of China (No. 61801407), China Scholarship Council (No. 201908515099), Fund of Robot Technology used for Special Environment Key Laboratory of Sichuan (No. 18kftk03), and Natural Science Foundation of Southwest University of Science and Technology (No. 17zx7110, 18zx7145).

CONFLICT OF INTEREST

The authors declare no known competing financial interests or personal relationships that influence the work reported in this paper.

DATA AVAILABILITY STATEMENT

The data that supports the results of this study is publicly available on ResearchGate: https://www.researchgate.net/project/Whole-Life-Cycle-Test and https://www.researchgate.net/project/Lithium-ion-Battery-Tests.

ORCID

Paul Takyi-Aninakwa https://orcid.org/0000-0001-8210-6340

Shunli Wang https://orcid.org/0000-0003-0485-8082

REFERENCES

1. Miniguano H, Barrado A, Lazaro A, Zumel P, Fernandez C. General parameter identification procedure and comparative study of Li-ion battery models. IEEE Trans. Veh. Technol. 2020; 69(1):235-245. doi:10.1109/TVT.2019.2952970

2. Espeda IB, Jinasena A, Burheim OS, Lamb JJ. Current trends for state-of-charge (SOC) estimation in lithium-ion battery electric vehicles. Energies. 2021;14(11):3284. doi:10.3390/en14113284

3. Liu F, Dai J. Equalization circuit topologies of lithium battery strings: a brief review. J Phys Conf Ser. 2020;1633:012141. doi: 10.1088/1742-6596/1633/1/012141

4. Ling L., Sun D., Yu X., Huang R. State of charge estimation of Lithium-ion batteries based on the probabilistic fusion of two kinds of cubature Kalman filters. J Energy Storage. 2021;43: 103070. doi:10.1016/j.est.2021.103070

5. Rzepka B, Bischof S, Blank T. Implementing an extended Kalman filter for SoC estimation of a Li-ion battery with hysteresis: a step-by-step guide. Energies. 2021;14(13):3733. doi:10.3390/en14133733

6. Naseri F, Karimi S, Farjah E, Schaltz E. Supercapacitor management system: A comprehensive review of modeling, estimation, balancing, and protection techniques. Renew Sustain Energy Rev. 2022;155:111913. doi:10.1016/j.rser.2021.111913

7. Ouyang Q, Ma R, Wu Z, Xu G, Wang Z. Adaptive square-root unscented Kalman filter-based state-of-charge estimation for lithium-ion batteries with model parameter online identification. Energies. 2020;13:4968. doi:10.3390/en13184968

8. Xing J, Wu P. State of charge estimation of lithium-ion battery based on improved adaptive unscented Kalman filter. Sustainability. 2021;13:5046. doi:10.3390/su13095046

9. Yang K, Tang Y, Zhang Z. Parameter identification and state-of-charge estimation for lithium-ion batteries using separated time scales and extended Kalman filter. Energies. 2021;14:1054. doi:10.3390/en14041054

10. Hu X, Xu L, Lin X, Pecht M. Battery lifetime prognostics. Joule. 2019;4(2):310-346. doi:10.1016/j.joule.2019.11.018

11. Ge D, Zhang Z, Kong X, Wan Z. Online SoC estimation of lithium-ion batteries using a new sigma points Kalman filter. Appl Sci. 2021;11(24):11797,. doi:10.3390/app112411797

12. Xin X, Wang SL, Fernandez C, Yu CM, Zou CY, Cong J. A novel practical state of charge estimation method: an adaptive improved ampere-hour method based on composite correction factor. Int J Energy Res. 2020;1-20:11385-11404. doi:10.1002/er.5758

13. Gong D, Gao Y, Kou Y. Parameter and state of charge estimation simultaneously for lithium-ion battery based on improved open circuit voltage estimation method. Energy Technol. 2021; 9:2100235. doi:10.1002/ente.202100235

14. Duan W, Song C, Peng S, Xiao F, Shao Y, Song S. An improved gated recurrent unit network model for state-of-charge estimation of lithium-ion battery. Energies. 2020;13:6366. doi:10.3390/en13236366

15. Chen Z, Zhao H, Shu X, Zhang Y, Shen J, Liu Y. Synthetic state of charge estimation for lithium-ion batteries based on long short-term memory network modeling and adaptive H-Infinity filter. Energy. 2021;228:120630. doi:10.1016/j.energy.2021.120630

16. Li M, Zhang Y, Hu Z, Zhang Y, Zhang J. A battery soc estimation method based on AFFRLS-EKF. Sensors. 2021;21:5698. doi:10.3390/s21175698

17. Kong X, Plett GL, Trimboli MS, et al. Pseudo-two-dimensional model and impedance diagnosis of micro internal short circuit in lithium-ion cells. J Energy Storage. 2020;27:101085. doi:10.1016/j.est.2019.101085

18. Li W, Demir I, Cao D, et al. Data-driven systematic parameter identification of an electrochemical model for lithium-ion batteries with artificial intelligence. Energy Storage Mater. 2022;44: 557-570. doi:10.1016/j.ensm.2021.10.023

19. Lai X, Wang S, He L, Zhou L, Zheng Y. A hybrid state-ofcharge estimation method based on credible increment for electric vehicle applications with large sensor and model errors. J Energy Storage. 2020;27:101106. doi:10.1016/j.est.2019.101106

20. Wu L, Liu K, Pang H, Jin J. Online SOC estimation based on simplified electrochemical model for lithium-ion batteries considering current bias. Energies. 2021;14:5265. doi:10.3390/en14175265

21. Khaki B, Das P. An equivalent circuit model for vanadium redox batteries via hybrid extended Kalman filter and particle filter methods. J Energy Storage. 2021;39:102587. doi:10.1016/j.est.2021.102587

22. Zheng Y, Shi Z, Guo D, Dai H, Han X. A simplification of the time-domain equivalent circuit model for lithium-ion batteries based on low-frequency electrochemical impedance spectra. J Power Sources. 2021;489:229505. doi:10.1016/j.jpowsour.2021.229505

23. Deng D, Wang S, Jin S, Fernandez C. A critical review of online battery remaining useful lifetime prediction methods. Front Mech Eng. 2021;7:719718. doi:10.3389/fmech.2021.719718

24. Li Y, Guo H, Qi F, Guo Z, Li M. Comparative study of the influence of open circuit voltage tests on state of charge online estimation for lithium-ion batteries. IEEE Access. 2020;8:17535-17547. doi:10.1109/ACCESS.2020.2967563

25. Bruch M, Millet L, Kowal J, Vetter M. Novel method for the parameterization of a reliable equivalent circuit model for the precise simulation of a battery cell's electric behavior. J Power Sources. 2021;490:229513. doi:10.1016/j.jpowsour.2021.229513

26. Jin G, Li L, Xu Y, Hu M, Fu C, Qin D. Comparison of SOC estimation between the integer-order model and fractional-order model under different operating conditions. Energies. 2020;13: 1785. doi:10.3390/en13071785

27. Wang H, Fan Y, Chen C, Tao T, Qiao Z. Novel estimation solution on lithium-ion battery state of charge with current-free detection algorithm. IET Circuits Devices Syst. 2019;13:245-249. doi:10.1049/iet-cds.2018.5406

28. Yang X, Wang S, Xu W, Qiao J, Yu C, Fernandez C. Fuzzy adaptive singular value decomposition cubature Kalman filtering algorithm for lithium-ion battery state-of-charge estimation. Int J Circuit Theory Appl. 2022;50:614-632.

29. Sun D, Yu X, Wang C, et al. State of charge estimation for lithium-ion battery based on an intelligent adaptive extended Kalman filter with improved noise estimator. Energy. 2021;214: 119025. doi:10.1016/j.energy.2020.119025

30. Shen X, Zhu W, Yang Y, Xie J, Huang L. A state of charge estimation method based on APSO-PF for lithium-ion battery. IEEE Fourth International Electrical and Energy Conference (CIEEC). Vol 2021. Wuhan, China: IEEE. 2021:1-6. doi:10.1109/CIEEC50170.2021.9510942

31. Lv J, Jiang B, Wang X, Liu Y, Fu Y. Estimation of the state of charge of lithium batteries based on adaptive unscented Kalman filter algorithm. Electronics. 2020;9:1425. doi:10.3390/electronics9091425

32. He L, Wang Y, Wei Y, Wang M, Hu X, Shi Q. An adaptive central difference Kalman filter approach for state of charge estimation by fractional order model of lithium-ion battery. Energy. 2022;244:122627. doi:10.1016/j.energy.2021.122627

33. Wang S, Fernandez C, Yu C, Fan Y, Cao W, Stroe D-I. A novel charged state prediction method of the lithium-ion battery packs based on the composite equivalent modelling and improved splice Kalman filtering algorithm. J Power Sources. 2020;471:228 450. doi:10.1016/j.jpowsour.2020.228450

34. Cong J, Wang S, Wu B, Fernandez C, Xin X, Coffie-Ken J. A state-of-charge estimation method of the power lithium-ion battery in complex conditions based on adaptive square root extended Kalman filter. Energy. 2021;219:119 603. doi:10.1016/j.energy.2020.119603

35. Yang S, Zhou S, Hua Y, et al. A parameter adaptive method for state of charge estimation of lithium-ion batteries with an improved extended Kalman filter. Sci Rep. 2021;11:5805. doi:10.1038/s41598-021-84729-1

36. Xu P, Li J, Sun C, Yang G, Sun F. Adaptive state-of-charge estimation for lithium-ion batteries by considering capacity degradation. Electronics. 2021;10:122. doi:10.3390/electronics10020122

37. Zhang S, Xu G, Zhang X. A novel one-way transmitted coestimation framework for capacity and state-of-charge of lithium-ion battery based on double adaptive extended Kalman filters. J Energy Storage. 2021;33:102 093. doi:10.1016/j.est.2020.102093

38. Yi J, Zhou X, Zhang J, Li Z. A hybrid method for SOC estimation of power battery. J Control Sci Eng. 2021;2021:6758679. doi:10.1155/2021/6758679

39. Zhang S, Zhang C, Jiang S, Zhang X. A comparative study of different adaptive extended/unscented Kalman filters for lithium-ion battery state-of-charge estimation. Energy. 2022; 246:123423. doi:10.1016/j.energy.2022.123423

40. Chen L, Chen Y, Lopes AM, Kong H, Wu R. State of charge estimation of lithium-ion batteries based on fuzzy fractional order unscented Kalman filter. Fractal Fract. 2021;5(3):91. doi: 10.3390/fractalfract5030091

41. Yang X, Wang S, Xu W, Qiao J, Yu C, Takyi-Aninakwa P. S. Jin, a novel fuzzy adaptive cubature Kalman filtering method for the state of charge and state of energy co-estimation of lithium-ion batteries. Electrochimica Acta. 2022;415:140241. doi:10.1016/j.electacta.2022.140241

42. Ma L, Xu Y, Zhang H, Yang F, Wang X, Li C. Co-estimation of state of charge and state of health for lithium-ion batteries based on fractional-order model with multi-innovations unscented Kalman filter method. J Energy Storage. 2022;52(Part B):104904. doi:10.1016/j.est.2022.104904

43. Xu H, Yuan H, Zou C, Li Z, Zhang L. Co-estimation of state of charge and state of health for lithium-ion batteries based on fractional-order calculus. IEEE Trans Veh Technol. 2018;67(11): 10319-10329. doi:10.1109/TVT.2018.2865664

44. Wu M, Qin L, Wu G. State of power estimation of power lithium-ion battery based on an equivalent circuit model. J Energy Storage. 2022;51:104538. doi:10.1016/j.est.2022.104538

45. She C, Zhang L, Wang Z, Sun F, Liu P, Song C. Battery state of health estimation based on incremental capacity analysis method: synthesizing from cell-level test to real-world application. IEEE J Emerg Sel Top Power Electron. 2021;99:1. doi:10.1109/JESTPE.2021.3112754

46. Wang Z, Song C, Zhang L, Zhao Y, Liu P, Dorrell DG. A data driven method for battery charging capacity abnormality diagnosis in electric vehicle applications. IEEE Trans Transport Electrification. 2022;8(1):990-999. doi:10.1109/TTE.2021.3117841

47. Wang Y-X, Chen Z, Zhang W. Lithium-ion battery state-ofcharge estimation for small target sample sets using the improved GRU-based transfer learning. Energy. 2022;244: 123178. doi:10.1016/j.energy.2022.123178

48. Li H, Wang S, Islam M, Bobobee ED, Zou C, Fernandez C. A novel state of charge estimation method of lithium-ion batteries based on the IWOA-AdaBoost-Elman algorithm. Int J Energy Res. 2022;46(4):5134-5151. doi:10.1002/er.7505

49. Jia M, Wang D, Qiu J. A GRU-RNN based momentum optimized algorithm for SOC estimation. J Power Sources. 2020; 459:228051. doi:10.1016/j.jpowsour.2020.228051

50. He L, Hu MK, Wei YJ, Liu BJ, Shi Q. State of charge estimation by finite difference extended Kalman filter with HPPC parameters identification. Sci China Techol. Sci. 2020;63:410-421. doi: 10.1007/s11431-019-1467-9

51. Wang Z, Feng G, Liu X, Gu F, Ball A. A novel method of parameter identification and state of charge estimation for lithium-ion battery energy storage system. Journal of Energy Storage. 2022;49:104124. doi:10.1016/j.est.2022.104124

52. Zhang F, Zhi H, Zhou P, et al. State of charge estimation of Liion battery for underwater vehicles based on EKF-RELM under temperature-varying conditions. Appl Ocean Res. 2021;114: 102802. doi:10.1016/j.apor.2021.102802

53. Ding X, Zhang D, Cheng J, Wang B, Luk PCK. An improved Thevenin model of lithium-ion battery with high accuracy for electric vehicles. Appl Energy. 2019;254:113615. doi:10.1016/j.apenergy.2019.113615

54. Yu Q, Wan C, Li JEL, Zhang X, Huang Y, Liu T. An open circuit voltage model fusion method for state of charge estimation of lithium-ion batteries. Energies. 1797;14:2021. doi:10.3390/en140717